Endothelium-protective sphingosine-1-phosphate provided by HDL-associated apolipoprotein M

Christina Christoffersen[a,1], Hideru Obinata[b,1], Sunil B. Kumaraswamy[c], Sylvain Galvani[b], Josefin Ahnström[c], Madhumati Sevvana[d], Claudia Egerer-Sieber[d], Yves A. Muller[d], Timothy Hla[b,2], Lars B. Nielsen[a,e,2], and Björn Dahlbäck[c,2]

[a]Department of Clinical Biochemistry, Rigshospitalet, 2100 Copenhagen, Denmark; [b]Center for Vascular Biology, Department of Pathology and Laboratory Medicine, Weill Cornell Medical College, Cornell University, New York, NY 10065; [c]Wallenberg Laboratory, Department of Laboratory Medicine, Skåne University Hospital, Lund University, SE 20502 Malmö, Sweden; [d]Department of Biology, Friedrich-Alexander-University Erlangen-Nuremberg, D-91052 Erlangen, Germany; and [e]Department of Biomedical Sciences, University of Copenhagen, 2100 Copenhagen, Denmark

Edited* by John A. Glomset, University of Washington, Seattle, WA, and approved May 4, 2011 (received for review February 25, 2011)

Protection of the endothelium is provided by circulating sphingosine-1-phosphate (S1P), which maintains vascular integrity. We show that HDL-associated S1P is bound specifically to both human and murine apolipoprotein M (apoM). Thus, isolated human ApoM$^+$ HDL contained S1P, whereas ApoM$^-$ HDL did not. Moreover, HDL in *Apom*$^{-/-}$ mice contains no S1P, whereas HDL in transgenic mice overexpressing human apoM has an increased S1P content. The 1.7-Å structure of the S1P–human apoM complex reveals that S1P interacts specifically with an amphiphilic pocket in the lipocalin fold of apoM. Human ApoM$^+$ HDL induced S1P$_1$ receptor internalization, downstream MAPK and Akt activation, endothelial cell migration, and formation of endothelial adherens junctions, whereas apoM$^-$ HDL did not. Importantly, lack of S1P in the HDL fraction of *Apom*$^{-/-}$ mice decreased basal endothelial barrier function in lung tissue. Our results demonstrate that apoM, by delivering S1P to the S1P$_1$ receptor on endothelial cells, is a vasculoprotective constituent of HDL.

endothelial function | crystal structure | sphingolipids | vascular permeability | atherosclerosis

Sphingosine-1-phosphate (S1P), the phosphorylated metabolite of D-sphingosine, binds to five G protein-coupled receptors (S1P$_1$–S1P$_5$) and regulates a plethora of biological actions (1–6). In particular, the prototypical S1P$_1$ receptor is essential for vascular maturation during development and promotes endothelial cell migration, angiogenesis, and barrier functions (7–9). Thus, S1P is required for maintenance of the barrier property of the lung endothelium (10). Plasma S1P, which is derived from several cellular sources (11, 12), is associated with HDL (~65%) and albumin (~35%) (3, 5). HDL-induced vasorelaxation as well as barrier-promoting and pro-survival actions on the endothelium have been attributed to S1P signaling (2, 4, 13). Hence, much of the endothelium-protective actions of HDL may result from the actions of S1P on the endothelial S1P receptors. However, the molecular nature of the S1P binding to HDL and interaction with S1P receptors has not been characterized.

Apolipoprotein M (apoM) is a lipocalin that resides mainly in the plasma HDL fraction (14). The retained hydrophobic NH_2-terminal signal peptide anchors apoM in the phospholipid layer of the lipoprotein and prevents filtration of the ~22-kDa protein in the kidney (15). The biological functions of apoM are understood only partly. Studies in apoM gene-modified mice suggest that apoM has antiatherogenic effects, possibly related in part to apoM's ability to increase cholesterol efflux from macrophage foam cells, to increased preβ-HDL formation, and to antioxidative effects (16–18). The recent elucidation of the crystal structure of human recombinant apoM (r-apoM) demonstrated a typical lipocalin fold characterized by an eight-stranded antiparallel β-barrel enclosing an internal binding pocket that probably facilitates binding of small lipophilic ligands (19). Indeed, r-apoM expressed in *Escherichia coli* was found to co-crystallize with myristic acid (19), illustrating that apoM can bind lipid compounds with fatty acid side chains, and in vitro binding experiments demonstrated that S1P displaced the myristic acid with an IC_{50} of 0.90 μM (19). We demonstrate here that apoM is the carrier of S1P in HDL, mediating vasoprotective actions on the endothelium.

Results and Discussion

To study the molecular basis of apoM interaction with S1P, we determined the crystal structure of N-terminally truncated human apoM (residues 22–188) (r-apoM) in complex with S1P at 1.7-Å resolution. S1P is bound at the center of the calyx-like ligand-binding pocket (Fig. 1 and Fig. S1). It participates in numerous specific interactions with apoM (Fig. 1 and Fig. S2). The phosphate moiety interacts directly with the side chains of Arg98, Arg116, and Trp100 (Fig. 1 and Fig. S2). The S1P amino group is hydrogen-bonded to Glu136 and to Tyr102 and Arg143 via bridging water molecules. The hydroxyl group of S1P interacts via a bridging water molecule with the hydroxyl group of Tyr147 (Fig. 1 and Fig. S2). The hydrocarbon chain of S1P points toward the interior of the calyx. Hence, its interaction with apoM and its location coincide with that of myristic acid in a previous complex (Figs. S2 and S3) (19). When all these binding interactions are considered together, the lipid-binding site of apoM is highly complementary to the structure of S1P. In particular, the recognition of the phosphate group by several arginines hints that the S1P–apoM interaction is very specific.

To elucidate whether apoM is the physiological carrier of HDL-associated S1P in vivo, plasma S1P was measured in apoM-knockout (*Apom*$^{-/-}$) mice and in two lines of human apoM transgenic mice having either twofold (*Apom-Tg*^{N}) or 10-fold (*Apom-Tg*^{H}) increased plasma apoM concentrations (17). Compared with WT mice, plasma S1P was reduced by 46% in *Apom*$^{-/-}$ mice ($P = 0.0007$) and was increased by 71% ($P = 0.0005$) and by 267% ($P = 0.0002$) in the *Apom-Tg*^{N} and *Apom-Tg*^{H} mice, re-

Author contributions: C.C., H.O., Y.A.M., T.H., L.B.N., and B.D. designed research; C.C., H.O., S.B.K., S.G., J.A., M.S., and C.E.-S. performed research; C.C., H.O., J.A., M.S., Y.A.M., T.H., L.B.N., and B.D. analyzed data; and C.C., H.O., Y.A.M., T.H., L.B.N., and B.D. wrote the paper.

The authors declare no conflict of interest.

*This Direct Submission article had a prearranged editor.

Freely available online through the PNAS open access option.

Data deposition: Crystallography, atomic coordinates, and structure factors for the S1P-apoM crystal structure have been deposited in the Protein Data Bank, www.pdb.org (PDB ID code 2YG2).

[1]C.C. and H.O. contributed equally to this work.

[2]To whom correspondence may be addressed. E-mail: tih2002@med.cornell.edu, larsbo@rh.dk, or bjorn.dahlback@med.lu.se.

This article contains supporting information online at www.pnas.org/lookup/suppl/doi:10.1073/pnas.1103187108/-/DCSupplemental.

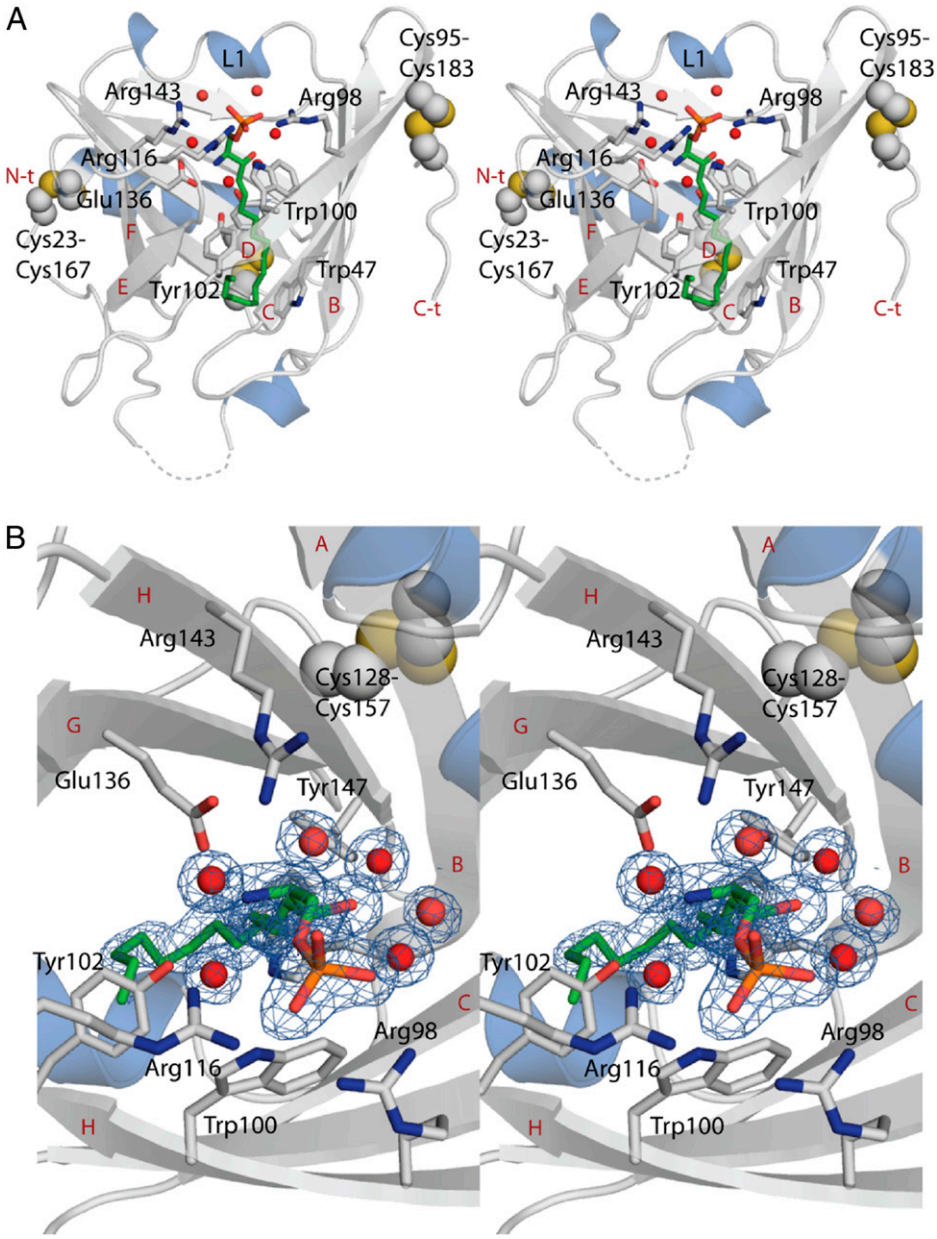

Fig. 1. The structure of the ApoM–S1P complex reveals the determinants of S1P-binding specificity. (*A*) Stereo view of the crystal structure of apoM with S1P at 1.7-Å resolution. S1P is shown as green sticks together with interacting residues. Strands B–F, the N terminus (*N*-t), and the C terminus (C-t) are labeled in red, and the interacting residues are labeled in black. (*B*) Top view of the S1P-binding site in close up. Electron density for S1P and surrounding water molecules is contoured at 1 σ and colored blue. Water molecules are shown as red spheres in both panels, and unmodeled loops toward the N terminus are shown as broken lines.

spectively (Fig. 2*A*). The plasma concentrations of HDL cholesterol, HDL total phospholipids, and apoA-I were affected only marginally in *Apom*$^{-/-}$ and *Apom-Tg*^{H} mice, demonstrating that the changes in S1P concentrations are related to apoM and not to variations in the amount of circulating HDL (17). When lipoproteins in WT mouse plasma were separated by gel filtration, the major peak of S1P coeluted with apoM in the HDL fractions, whereas a minor S1P peak coeluted with albumin (Fig. 2*B*). *Apom*$^{-/-}$ mice lacked S1P in the HDL fraction, but the S1P peak in the albumin fractions was present (Fig. 2*B*). *Apom-Tg*^{H} mice had increased S1P in HDL (Fig. 2*B*). This S1P was associated with apoM-containing HDL, as demonstrated by a parallel shift in S1P- and human apoM-elution profiles when a specific monoclonal antibody against human apoM (M58) was added to the plasma before gel filtration (Fig. S4 *A* and *B*).

Importantly, the amount of apoM in HDL is sufficient to accommodate and account for all HDL-bound S1P. The average plasma apoM concentration is similar in mice and humans, i.e., ∼0.9 μmol/L (17). Hence, the apparent molar ratio between HDL-bound S1P and plasma apoM is ∼1:3 in WT and *Apom-Tg*^{N} mice and ∼1:6 in *Apom-Tg*^{H} mice. On gel filtration of human plasma, the majority of S1P coeluted with HDL, indicating that in humans, also, the main part of lipoprotein-bound S1P is associated with HDL (Fig. S4*C*). When human HDL was separated by affinity chromatography into apoM^{+} HDL and apoM^{-} HDL fractions, S1P was found exclusively in apoM^{+} HDL (Fig. 2*C*). These data indicate that S1P in HDL is bound to apoM in both

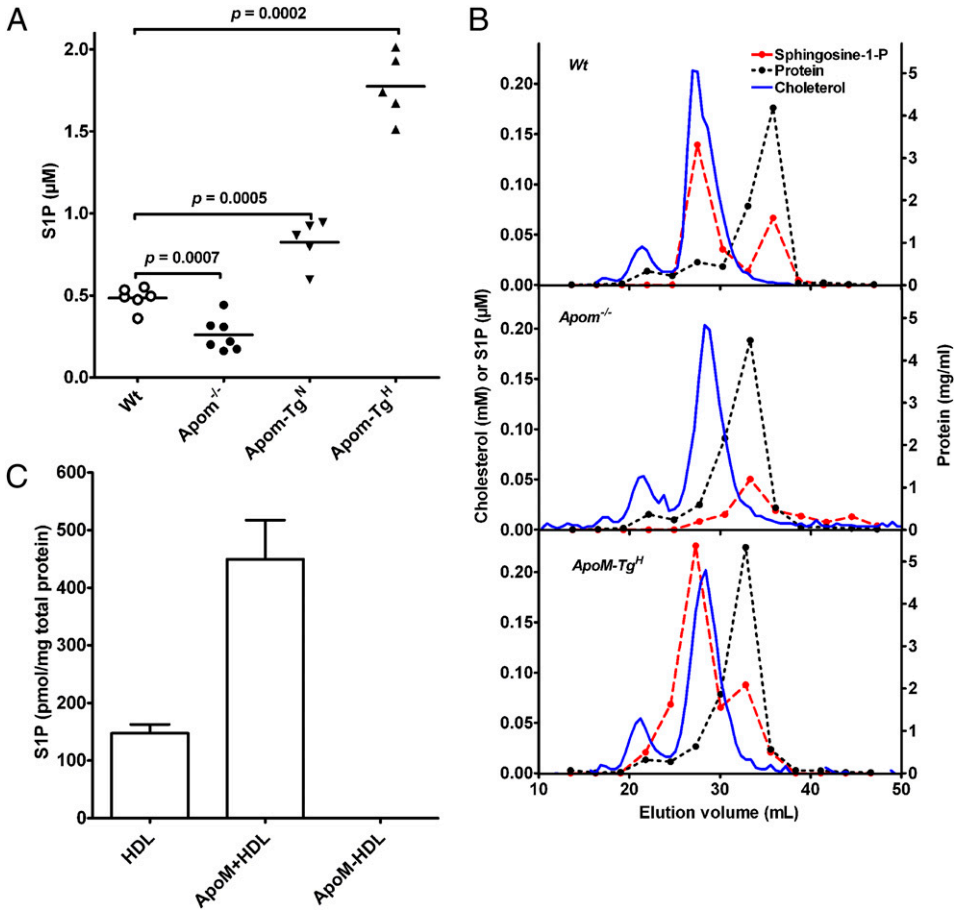

Fig. 2. *ApoM* gene dosage determines plasma S1P in genetically modified mice. (*A*) Plasma S1P in WT, *Apom*$^{-/-}$, and apoM-transgenic female mice with ~twofold (*Apom-Tg*^{N}) and ~10-fold (*Apom-Tg*^{H}) increased plasma apoM. Each point represents data from an individual mouse; horizontal lines indicate means. (*B*) Lipoproteins in pools of plasma from WT (*Top*), *Apom*$^{-/-}$ (*Middle*), or *Apom-Tg*^{H} (*Bottom*) mice were separated by gel filtration on serially connected Superose 6 and 12 columns. The flow rate was 0.4 mL/min. Fractions of 275 μL were collected. Aliquots of 10 consecutive fractions were pooled before measuring S1P (red filled symbols) and protein (dotted black line). Cholesterol concentration (solid blue line) was determined in each fraction. The scale bar for cholesterol (mmol/L) and S1P (μmol/L) is shown on the left *y* axis. Protein (mg/mL) is shown on the right *y* axis. (*C*) S1P was measured with HPLC in purified preparations of human total HDL, apoM^{+} HDL, and apoM^{-} HDL. Values are mean ± SEM (n = 3). S1P was not detectable in apoM^{-} HDL. Results were confirmed by LC-MS/MS.

humans and mice. Intrinsic fluorescence binding studies of human r-apoM showed that apoM can bind S1P with an IC_{50} of 0.9 μM (19). With the same experimental setup but using murine r-apoM, an IC_{50} for S1P of 0.95 ± 0.05 μM (n = 3) was obtained (Fig. S5), further supporting the idea that apoM is the physiological carrier of HDL-associated S1P.

The biological effects of S1P are mediated by activation of the G protein-coupled S1P receptors, leading to activation of downstream effectors such as p44/42, MAPK, and Akt (20). To assess whether apoM^{+} HDL and apoM-bound S1P can activate the $S1P_1$ receptor, we performed a ligand-induced receptor internalization assay in HEK293 cells stably expressing the GFP-tagged $S1P_1$ receptor (21). Both ApoM^{+} HDL and r-apoM–bound S1P induced robust internalization of GFP-$S1P_1$ receptor, similarly to albumin-bound S1P that was used as a positive control (Fig. 3*A*). Neither apoM^{-} HDL nor r-apoM without S1P caused receptor internalization. These data indicate that the apoM–S1P complex can activate the $S1P_1$ receptor, whether it is part of an HDL particle or not.

To test activation of endogenous $S1P_1$ receptors and the downstream signaling by apoM-bound S1P, human umbilical vein endothelial cells (HUVEC) were stimulated with various carriers complexed or not with S1P. Prominent phosphorylation of p44/42 and Akt was induced by apoM^{+} HDL but not by apoM^{-} HDL (Fig. 3*B*). Moreover, blocking of $S1P_1$ receptors with the $S1P_1$-selective antagonist VPC44116 (22, 23) essentially abolished the effect of apoM^{+} HDL on p44/42 and Akt phosphorylation (Fig. 3*B*), indicating that the effects of apoM^{+} HDL were mediated by the $S1P_1$ receptor. Albumin-bound S1P, apoM^{+} HDL and apoM-bound S1P showed similar time courses and dose responses in the activation of p44/42 and Akt (Fig. S6 *A* and *B*).

S1P is a potent chemoattractant for endothelial cells, which are essential for wound-healing response and angiogenesis (9, 24). ApoM^{+} HDL stimulated chemotaxis of HUVEC, and this effect was abolished by pretreatment with the $S1P_1$ antagonist VPC44116 (Fig. 3*C*). Both albumin- and r-apoM–bound S1P worked as chemoattractants in a concentration-dependent manner, but r-apoM–bound S1P showed slightly higher activity, especially at lower S1P concentrations (Fig. S6*C*). S1P suppresses abnormal vascular permeability by inducing the assembly of vascular endothelial (VE)-cadherin–containing adherens junctions between endothelial cells (1, 9). As shown in Fig. 3*D*, HUVEC were well spread, contained F-actin,and formed adherens junctions when treated with apoM^{+} HDL and with albumin- and r-apoM–bound S1P. In contrast, adherens junctions and F-actin were not induced efficiently by apoM^{-} HDL or by r-apoM without S1P.

The importance of S1P in regulating vascular integrity in vivo has been shown in mice lacking plasma S1P (10). These mice

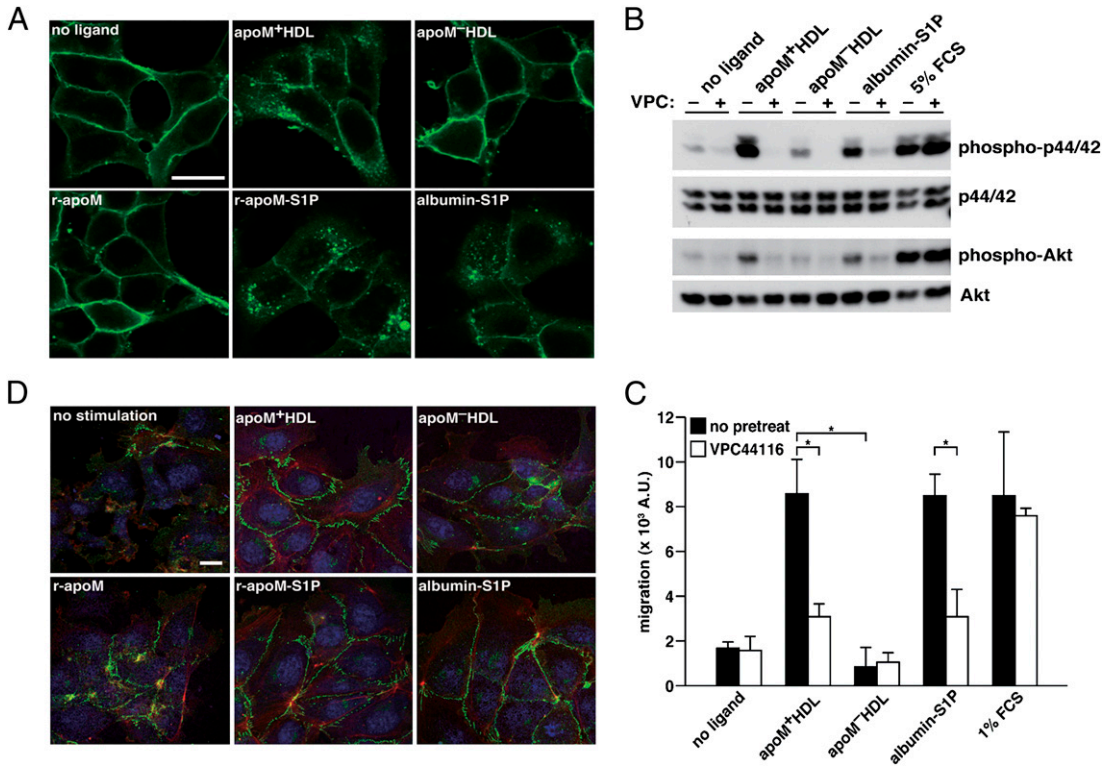

Fig. 3. ApoM-bound S1P activates $S1P_1$-mediated intracellular signaling pathways. (*A*) Confocal microscopy of HEK293 cells stably expressing $S1P_1$-GFP. Cells were serum starved, stimulated for 1 h with indicated ligands, fixed, and imaged. $ApoM^+$ HDL (equivalent to ~100 nM S1P as determined by LC/MS/MS) or $ApoM^-$ HDL was used at 100 μg/mL Fatty acid-free BSA and r-apoM were complexed with S1P and used at afinal concentration of 100 nM (equimolar for both protein and lipid). (Scale bar, 20 μm.) (*B*) HUVEC were serum starved and pretreated with 1 μM of the $S1P_1$ antagonist VPC44116 for 30 min before stimulated with $apoM^+$ HDL (20 μg/mL protein, 20 nM S1P), $apoM^-$HDL (20 μg/mL protein), or albumin-S1P (100 nM S1P and equimolar protein) for 10 min. (Note that VPC44116 has no inhibitory effects on cells stimulated by FCS, because FCS can activate receptor systems other than $S1P_1$.) Activation of p44/42 and Akt was examined by Western blot analysis using phospho-specific antibodies. (*C*) HUVEC were serum starved and pretreated with 1 μM VPC44116 for 30 min where indicated and subjected to migration assay with 10 μg/mL $apoM^+$ HDL (10 nM S1P), 10 μg/mL $apoM^-$ HDL, or 10 nM albumin-S1P. Data are mean ± SD ($n = 3$). *$P < 0.01$. (*D*) Microscopy of HUVEC that were serum starved and stimulated with 100 μg/mL $apoM^+$ HDL, $apoM^-$ HDL, 100 nM albumin-S1P, r-apoM–S1P, or 100 nM S1P-free r-apoM for 1 h. After fixation, VE-cadherin (green), nuclei (blue), and F-actin (red) were visualized with confocal microscopy. (Scale bar, 20 μm.)

extravasate albumin in their lungs, as demonstrated by i.v. injection of Evans Blue. After i.v. injection of Evans Blue, increased extravasation of Evans Blue in the lung was observed in the $Apom^{-/-}$ mice compared with WT and $Apom\text{-}Tg^H$ mice (Fig. 4). This observation suggests that, even though $Apom^{-/-}$ mice have albumin-bound S1P in the circulation, this S1P cannot fully maintain the endothelial barrier function in the lung. However, the increased vascular leakage in the $Apom^{-/-}$ mice was not followed by general edema, because the weight of the lung tissue was unchanged in the different strains of mice (Fig. S7).

Taken together, our data demonstrate that apoM is the physiological carrier protein of S1P in HDL and that apoM can deliver S1P to the $S1P_1$ receptor on endothelial cells. Thus, apoM-bound S1P mediates $S1P_1$ receptor activation, resulting in downstream (junction assembly) effects that are vasoprotective. These observations provide important information about the function of apoM and increase the understanding of the antiatherogenic effects of apoM demonstrated in several different mouse models (17, 18, 25). Atherosclerosis is a chronic inflammatory disease characterized by accumulation of oxidized lipoproteins and cholesterol-filled foam cells in the arterial intima. HDL can protect against atherosclerosis by pleiotropic mechanisms, e.g., by promoting cholesterol efflux from foam cells, by attenuating LDL oxidation, by anti-inflammatory or antiplatelet effects, and by protecting the endothelium. Although apoM enhances the antioxidant function of HDL and the ability of HDL to stimulate cholesterol efflux from foam cells, these antiatherogenic effects also are characteristics of apoM-free HDL (16, 17). In contrast, the S1P-mediated vasoprotective effects of HDL are unique, because apoM is the physiological carrier protein for S1P in HDL, and the subset of HDL that contains apoM mediates multiple S1P-dependent effects of HDL (1). However, in addition to the now-

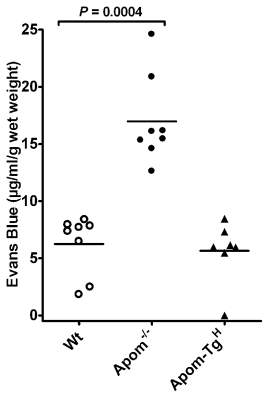

Fig. 4. The apoM–S1P complex maintains lung endothelial barrier function. WT, $Apom^{-/-}$, and $Apom\text{-}Tg^H$ mice were injected i.v. with Evans Blue (30 μg/g body weight). After 30 min the mice were perfused with saline; then the lungs were removed and used for extraction of Evans Blue. Each point represents the content of Evans Blue in the lungs of one mouse, and horizontal lines represent mean values.

reported effects on HDL functionality, apoM also has putatively proatherogenic effects on the metabolism of very low-density lipoprotein (VLDL)/LDL. Hence, the concentrations of apoM and LDL cholesterol in human plasma correlate positively (26), and in mice the overexpression of human apoM delays the clearance of VLDL/LDL, resulting in increased plasma concentrations of VLDL/LDL (25). Thus, adverse effects on LDL metabolism may counteract the beneficial effects on vascular endothelium of HDL-associated apoM. These dual effects would agree with the lack of association between plasma apoM levels and the risk of coronary heart disease observed in human case-control studies (27).

Many effects on endothelial cells have been attributed to S1P in plasma. Recently, Camerer et al. (10) showed that plasma S1P plays an important role in maintaining vascular barrier function. Our in vivo data further support the conclusion that plasma S1P is essential in maintaining vascular integrity. However, the presence of S1P bound to albumin in plasma is not sufficient, because our results demonstrate that S1P carried by apoM in the HDL fraction has an important role in preserving vascular integrity. Thus, even though the estimated concentration of albumin-bound S1P is sufficient to activate the S1P receptors in the *Apom*$^{-/-}$ mice, these mice have decreased endothelial barrier function in the lung. Because apoM determines the S1P-binding capacity of HDL, we propose that elevation of apoM^{+} HDL would be vasoprotective by preventing endothelial injury, allowing endothelial regeneration, and maintaining vascular integrity.

Our results raise the interesting question of how S1P is delivered from apoM to S1P receptors. The specific anchoring of apoM to lipoproteins and in particular to HDL by its retained signal peptide suggests that association of apoM with HDL and lipids in general is an important component for its function. The structural elucidation of the apoM–S1P complex revealed several features that possibly promote S1P uptake or release upon membrane or even receptor associations. In the two complexes of apoM with S1P or myristic acid, the peptide segment preceding the first β-strand of the lipocalin fold adopts multiple conformations, thereby changing the exposure of several hydrophobic amino acids, partially uncovering the bottom of the binding calyx, and possibly facilitating ligand release (Fig. S3). Equally possible, a previously observed weak point in the apoM barrel structure (between strands D and G) (28) could facilitate a lateral release of the ligand from the calyx upon docking to membranes or even to the $S1P_1$ receptors. Although these scenarios currently remain hypothetical, r-apoM clearly is capable of delivering S1P to $S1P_1$ receptors at the cell surface. It remains to be tested whether apoM is equally effective in delivering S1P to other S1P receptors ($S1P_{2–5}$) or if the S1P binding to apoM provides receptor specificity that directs the biological effects of HDL-associated S1P.

In summary, our studies define apoM as a carrier of S1P in HDL and demonstrate that the HDL-associated apoM–S1P complex mediates vasoprotective actions on the endothelium. This signaling axis may be critical in normal vascular homeostasis and perturbed in vascular diseases.

Materials and Methods

Detailed descriptions of materials and methods are given in *SI Materials and Methods*.

Mice. *Apom-Tg*^{N}, *Apom-Tg*^{H}, and *Apom*$^{-/-}$ mice were backcrossed at least seven times with *C57B6/J* mice. Mice were housed at the Panum Institute, University of Copenhagen, Copenhagen (17, 25).

Lipoproteins and S1P. Human apoM^{+} HDL and apoM^{-} HDL were isolated from human plasma with ultracentrifugation (1.063–1.21 g/L) followed by immunoaffinity chromatography on an anti-apoM monoclonal column (16). ApoM was quantified with ELISA (26). For gel filtration, 500-μL plasma samples from *Apom-Tg*^{H} (n = 5), *Apom*$^{-/-}$ (n = 7), and WT (n = 6) mice were separated on serially connected Superose 6 and Superose 12 10/300 GL columns (16). S1P was measured with HPLC (29) or liquid chromatography tandem MS (LC-MS/MS) (30).

Western Blotting. Western blotting was done after separation in 10 or 12% SDS/PAGE gels with antibodies against human apoM, p44/42, phospho-p44/42, and phospho-Akt (Cell Signaling).

Crystal Structure of r-ApoM with S1P. Human r-apoM was prepared as described (15). The r-apoM–S1P complex was prepared by adding S1P (dry powder) to a concentrated solution of r-apoM (13 mg/mL). Formation of the r-apoM–S1P complex could be monitored with isoelectric focusing (Fig. S8*A*). The r-apoM–S1P complex was purified by gel filtration to remove unbound S1P before crystallization using hanging-drop vapor diffusion. Data were collected to a resolution of 1.7 Å. The structure was solved using molecular replacement and refined to R-work and R-free of 19.1% and 22.1%, respectively (Table S1).

r-ApoM– and Albumin-Bound S1P. S1P was dissolved in methanol. After evaporation, the S1P was redissolved by sonication in 20 mM Tris-HCl (pH 8.0) containing equimolar amounts of r-apoM (19) or fatty acid free BSA (Sigma A6003) and kept at 4 °C until use.

Cell Culture. Passage 4–10 HUVEC were cultured as described (31). HEK293 cells stably expressing $S1P_1$-GFP (21) were cultured in DMEM with 10% FBS. Confocal laser scanning microscopy was performed using a FluoView FV10i system (Olympus). Migration assays were performed using a 96-well chemotaxis chamber system (Neuroprobe) (32). VE-cadherin was visualized with immunofluorescence, nuclei with TO-PRO-3 dye, and F-actin with rhodamine phalloidin.

Vascular Permeability. Mice were injected i.v. with Evans Blue (30 μg/g body weight). After 30 min the mice were anesthetized and perfused extensively with saline via the right ventricle to remove intravascular Evans Blue. The lung wet weights were measured, and Evans Blue was extracted in 1 mL formamide at 56 °C for 16 h. Evans Blue concentration was determined from the OD_{620} minus OD_{500} in the extract and a serial dilution of a standard.

Statistics. Numerical differences were analyzed with two-tailed Student's t test.

ACKNOWLEDGMENTS. We thank Karen Rasmussen and Charlotte Wandel and Bernd Gardill for technical assistance, Uwe Müller for help during diffraction data collection, and Dr. Kevin R. Lynch for the gift of VPC44116. This work was supported by Grant 07143 from the Swedish Research Council and by grants from the Söderberg's Foundation and the Swedish Heart-Lung Foundation (to B.D.), by Grants 09-06452/FSS (to L.B.N.) and 09-073571/FSS (to C.C.) from the Danish National Research Council, by grants from the Rigshospitalet Research Council (to L.B.N.) and from the Sonderfonds of the University Erlangen-Nuremberg (to Y.A.M.), and by Grants HL-67330, HL-70694, and HL89934 from the National Institutes of Health (to T.H.).

1. Garcia JG, et al. (2001) Sphingosine 1-phosphate promotes endothelial cell barrier integrity by Edg-dependent cytoskeletal rearrangement. *J Clin Invest* 108: 689–701.
2. Kimura T, et al. (2006) Role of scavenger receptor class B type I and sphingosine 1-phosphate receptors in high density lipoprotein-induced inhibition of adhesion molecule expression in endothelial cells. *J Biol Chem* 281:37457–37467.
3. Aoki S, et al. (2005) Sphingosine 1-phosphate-related metabolism in the blood vessel. *J Biochem* 138:47–55.
4. Nofer JR, et al. (2004) HDL induces NO-dependent vasorelaxation via the lysophospholipid receptor S1P3. *J Clin Invest* 113:569–581.
5. Argraves KM, Argraves WS (2007) HDL serves as a S1P signaling platform mediating a multitude of cardiovascular effects. *J Lipid Res* 48:2325–2333.
6. Ishii I, Fukushima N, Ye X, Chun J (2004) Lysophospholipid receptors: Signaling and biology. *Annu Rev Biochem* 73:321–354.
7. Liu Y, et al. (2000) Edg-1, the G protein-coupled receptor for sphingosine-1-phosphate, is essential for vascular maturation. *J Clin Invest* 106:951–961.
8. Paik JH, Chae Ss, Lee MJ, Thangada S, Hla T (2001) Sphingosine 1-phosphate-induced endothelial cell migration requires the expression of EDG-1 and EDG-3 receptors and Rho-dependent activation of alpha vbeta3- and beta1-containing integrins. *J Biol Chem* 276:11830–11837.

9. Lee MJ, et al. (1999) Vascular endothelial cell adherens junction assembly and morphogenesis induced by sphingosine-1-phosphate. *Cell* 99:301–312.
10. Camerer E, et al. (2009) Sphingosine-1-phosphate in the plasma compartment regulates basal and inflammation-induced vascular leak in mice. *J Clin Invest* 119: 1871–1879.
11. Pappu R, et al. (2007) Promotion of lymphocyte egress into blood and lymph by distinct sources of sphingosine-1-phosphate. *Science* 316:295–298.
12. Venkataraman K, et al. (2008) Vascular endothelium as a contributor of plasma sphingosine 1-phosphate. *Circ Res* 102:669–676.
13. Argraves KM, et al. (2008) High density lipoprotein-associated sphingosine 1-phosphate promotes endothelial barrier function. *J Biol Chem* 283:25074–25081.
14. Xu N, Dahlbäck B (1999) A novel human apolipoprotein (apoM). *J Biol Chem* 274: 31286–31290.
15. Christoffersen C, et al. (2008) The signal peptide anchors apolipoprotein M in plasma lipoproteins and prevents rapid clearance of apolipoprotein M from plasma. *J Biol Chem* 283:18765–18772.
16. Christoffersen C, et al. (2006) Isolation and characterization of human apolipoprotein M-containing lipoproteins. *J Lipid Res* 47:1833–1843.
17. Christoffersen C, et al. (2008) Effect of apolipoprotein M on high density lipoprotein metabolism and atherosclerosis in low density lipoprotein receptor knock-out mice. *J Biol Chem* 283:1839–1847.
18. Wolfrum C, Poy MN, Stoffel M (2005) Apolipoprotein M is required for prebeta-HDL formation and cholesterol efflux to HDL and protects against atherosclerosis. *Nat Med* 11:418–422.
19. Sevvana M, et al. (2009) Serendipitous fatty acid binding reveals the structural determinants for ligand recognition in apolipoprotein M. *J Mol Biol* 393:920–936.
20. Morales-Ruiz M, et al. (2001) Sphingosine 1-phosphate activates Akt, nitric oxide production, and chemotaxis through a Gi protein/phosphoinositide 3-kinase pathway in endothelial cells. *J Biol Chem* 276:19672–19677.
21. Liu CH, et al. (1999) Ligand-induced trafficking of the sphingosine-1-phosphate receptor EDG-1. *Mol Biol Cell* 10:1179–1190.
22. Oo ML, et al. (2007) Immunosuppressive and anti-angiogenic sphingosine 1-phosphate receptor-1 agonists induce ubiquitinylation and proteasomal degradation of the receptor. *J Biol Chem* 282:9082–9089.
23. Awad AS, et al. (2006) Selective sphingosine 1-phosphate 1 receptor activation reduces ischemia-reperfusion injury in mouse kidney. *Am J Physiol Renal Physiol* 290: F1516–F1524.
24. English D, et al. (2000) Sphingosine 1-phosphate released from platelets during clotting accounts for the potent endothelial cell chemotactic activity of blood serum and provides a novel link between hemostasis and angiogenesis. *FASEB J* 14: 2255–2265.
25. Christoffersen C, et al. (2010) Opposing effects of apolipoprotein m on catabolism of apolipoprotein B-containing lipoproteins and atherosclerosis. *Circ Res* 106:1624–1634.
26. Axler O, Ahnström J, Dahlbäck B (2007) An ELISA for apolipoprotein M reveals a strong correlation to total cholesterol in human plasma. *J Lipid Res* 48:1772–1780.
27. Ahnström J, et al. (2008) Levels of apolipoprotein M are not associated with the risk of coronary heart disease in two independent case-control studies. *J Lipid Res* 49: 1912–1917.
28. Sevvana M, et al. (2010) Mouse ApoM displays an unprecedented seven-stranded lipocalin fold: Folding decoy or alternative native fold? *J Mol Biol* 404:363–371.
29. He X, Huang CL, Schuchman EH (2009) Quantitative analysis of sphingosine-1-phosphate by HPLC after napthalene-2,3-dicarboxaldehyde (NDA) derivatization. *J Chromatogr B Analyt Technol Biomed Life Sci* 877:983–990.
30. Bielawski J, et al. (2009) Comprehensive quantitative analysis of bioactive sphingolipids by high-performance liquid chromatography-tandem mass spectrometry. *Methods Mol Biol* 579:443–467.
31. Hla T, Maciag T (1990) An abundant transcript induced in differentiating human endothelial cells encodes a polypeptide with structural similarities to G-protein-coupled receptors. *J Biol Chem* 265:9308–9313.
32. Michaud J, Im DS, Hla T (2010) Inhibitory role of sphingosine 1-phosphate receptor 2 in macrophage recruitment during inflammation. *J Immunol* 184:1475–1483.

Supporting Information

Christoffersen et al. 10.1073/pnas.1103187108

SI Materials and Methods

Mice. Mice were housed at the Panum Institute, University of Copenhagen, Copenhagen, and fed standard chow (Altromin 1314). *Apom-Tg*^{N}, *Apom-Tg*^{H}, or *Apom*$^{-/-}$ female mice were backcrossed more than seven times with *C57B6/J* mice (1, 2). WT mice were *Apom-Tg* littermates. Blood taken from the orbital venous plexus was placed in tubes containing ethylenediaminetetraacetic acid, kept on ice until plasma was isolated, and frozen in N_2 before storage at −80 °C. All procedures were approved by the Animal Experiments Inspectorate, Ministry of Justice, Denmark.

HPLC-Based Quantification of Sphingosine-1-Phosphate. For HPLC-based quantification of sphingosine-1-phosphate (S1P) (3), plasma (25 μL), isolated human HDL fractions (150 μL), or gel filtration fractions (500 μL) were supplemented with 25 ng of an internal standard [D-erythro-sphingosine-1-phosphate (C17 base), Avanti; iNstruchemie]. The S1P-containing phase was isolated with chloroform-methanol extractions in a two-step procedure followed by derivatization with 2,3-naphthalenedicarboxaldehyde. One microliter of the derivatized sample was analyzed with an Agilent 1290 HPLC (Agilent Technologies) using a Synergi 4u Fusion-RP 80A column (30 × 2.0 mm; Phenomenex) with a flow of 0.5 mL/min. Separation was performed using a gradient of the mobile phase: 0–6 min, 47.5%; 6–9 min, 47.5–87.5%; 9–10 min, 87.5%; 10–12, min 87.5–47.5%; and 12–15 min, 47.5%. The mobile phase consisted of acetonitrile (HPLC grade; Rathburn Chemicals Ltd), and the aqueous phase consisted of 20 mM potassium phosphate (KH2PO4, pH 4.8, HPLC grade; Sigma-Aldrich), each supplemented with 15% methanol (HPLC grade; Sigma-Aldrich). Results were confirmed with an independent HPLC method and by liquid chromatography-tandem MS (4).

Determination of ApoM Crystal Structure. The apolipoprotein M (apoM)–S1P complex was prepared by adding 0.5 mg of solid S1P (Sigma-Aldrich) to a solution of apoM containing myristic acid (120 μL of 13 mg/mL ApoM in 20 mM Tris/HCl, pH 7.2) (5) and was incubated at 0 °C for 4 wk. Successful complex formation was verified by isoelectric focusing (Fig. S8*A*). Excess S1P and fatty acids were removed by gel filtration, and the purified apoM–S1P complex then was concentrated to 13 mg/mL in a buffer of 20 mM Tris (pH 7.2) before crystallization. Crystallization conditions were screened with a Phoenix automated setup (Art Robbins) using PEG/Ion Screen and PEGRx crystallization kits (Hampton Research) in 96-well Greiner plates with a drop volume 0.4 μL and a protein:crystallization reagent ratio of 1:1 at 20 °C. An initial hit was obtained with 0.15 M lithium sulfate monohydrate, 0.1 M citric acid (pH 3.5), and 18% (wt/vol) PEG 6000. The crystals were reproduced using the same conditions and the hanging-drop vapor diffusion method (6). Crystals were flash frozen in liquid nitrogen using 15% ethylene glycol as a cryoprotectant, and native data sets were collected at the BESSY synchrotron in Berlin at 100 K. The diffraction data were processed using the programs XDS and XSCALE (7). The protein crystallized in space group $P3_121$ with two molecules in the asymmetric unit. Crystals diffracted to a maximum resolution of 1.7 Å. The structure was solved by molecular replacement using the program PHASER (8) and the published human apoM structure (PDB ID: 2WEW) as a search model. The ligand S1P could be identified unambiguously in difference Fourier electron density maps (Fig. S8 *B–D*). The model was refined to an R_{work} and R_{free} of 19.1 and 22.1%, respectively, using the program REFMAC (9) and alternating with model building using COOT (10). The data quality and the final refinement statistics are shown in Table S1. The structure was validated using the program PROCHECK (11) and illustrated using PYMOL (12). The PDB accession code for the structure is 2YG2.

Binding of S1P to Recombinant Mouse ApoM. Intrinsic fluorescence quenching was studied after addition of S1P to 0.7 μM murine recombinant apoM (r-apoM) (5). Because it is possible that murine r-apoM binds and contains myristic acid in a manner similar to that of its human counterpart (5), the binding data are reported as IC_{50} values. This approach also allows S1P binding to murine r-apoM to be compared directly with the previous data on human apoM–S1P binding.

Cell Culture. Passage 4–10 human umbilical vein endothelial cells (HUVEC) (13) and HEK293 cells stably expressing S1P receptor 1 ($S1P_1$)-GFP (14) were cultured as described. HUVEC cells were serum starved and pretreated with 1 μM VPC4416 for 30 min where indicated (15).

Migration Assay. Migration assays were performed using a 96-well chemotaxis chamber system (Neuroprobe) (16). After serum starvation for 3 h in M199 medium, HUVEC were placed in the upper well of the chemotaxis chamber at a density of 1×10^5 cells per well and were allowed to migrate toward chemoattractants in the lower well, which was separated from the upper well by a fibronectin-coated polycarbonate filter with 8-μm pores. After incubation for 4 h at 37 °C, the upper surface of the filter was wiped clean of nonmigrating cells, and the cells on the lower surface were stained by 1% crystal violet. The filter was scanned, and the color density of each well was quantified using ImageJ software.

$S1P_1$ Internalization Assay. HEK293 cells stably expressing $S1P_1$-GFP were plated on 35-mm glass-bottomed dishes and were serum starved for 24 h in DMEM containing 2% charcoal-stripped serum followed by starvation for another 2 h in plain DMEM, stimulated as indicated, and fixed with 4% paraformaldehyde. Confocal laser-scanning microscopy analysis was performed using a FluoView FV10i system (Olympus).

Vascular Endothelial Cadherin Immunostaining. HUVEC were plated on 35-mm glass-bottomed dishes and serum starved for 24 h in M199 medium containing 1% charcoal-stripped serum. The cells were serum starved for another 2 h in plain M199 medium, stimulated as indicated, and fixed with 4% paraformaldehyde. Immunofluorescence analysis was performed using anti-vascular endothelial cadherin antibody (Santa Cruz) and Alexa Fluor 488-conjugated secondary antibody (Invitrogen). Nuclei were stained with TO-PRO-3 dye (Invitrogen). Confocal laser-scanning microscopy analysis was performed as mentioned above.

1. Christoffersen C, et al. (2008) Effect of apolipoprotein M on high density lipoprotein metabolism and atherosclerosis in low density lipoprotein receptor knock-out mice. *J Biol Chem* 283:1839–1847.
2. Christoffersen C, et al. (2010) Opposing effects of apolipoprotein m on catabolism of apolipoprotein B-containing lipoproteins and atherosclerosis. *Circ Res* 106: 1624–1634.
3. He X, Huang CL, Schuchman EH (2009) Quantitative analysis of sphingosine-1-phosphate by HPLC after napthalene-2,3-dicarboxaldehyde (NDA) derivatization. *J Chromatogr B Analyt Technol Biomed Life Sci* 877:983–990.
4. Bielawski J, et al. (2009) Comprehensive quantitative analysis of bioactive sphingolipids by high-performance liquid chromatography-tandem mass spectrometry. *Methods Mol Biol* 579:443–467.

5. Sevvana M, et al. (2009) Serendipitous fatty acid binding reveals the structural determinants for ligand recognition in apolipoprotein M. *J Mol Biol* 393:920–936.
6. McPherson A (1990) Current approaches to macromolecular crystallization. *Eur J Biochem* 189:1–23.
7. Kabsch W (1993) Automatic processing of rotation differafction data from crystals of initially unknown symmetry and cell constants. *J Appl Cryst* 26:795–800.
8. McCoy AJ, et al. (2007) Phaser crystallographic software. *J Appl Cryst* 40:658–674.
9. Murshudov GN, Vagin AA, Dodson EJ (1997) Refinement of macromolecular structures by the maximum-likelihood method. *Acta Crystallogr D Biol Crystallogr* 53:240–255.
10. Emsley P, Cowtan K (2004) Coot: Model-building tools for molecular graphics. *Acta Crystallogr D Biol Crystallogr* 60:2126–2132.
11. Laskowski RA, Moss DS, Thornton JM (1993) Main-chain bond lengths and bond angles in protein structures. *J Mol Biol* 231:1049–1067.
12. DeLano W (2003) *The PyMOL Molecular Graphic System* (DeLano Scientific LLC, San Carlos, CA).
13. Hla T, Maciag T (1990) An abundant transcript induced in differentiating human endothelial cells encodes a polypeptide with structural similarities to G-protein-coupled receptors. *J Biol Chem* 265:9308–9313.
14. Liu CH, et al. (1999) Ligand-induced trafficking of the sphingosine-1-phosphate receptor EDG-1. *Mol Biol Cell* 10:1179–1190.
15. Oo ML, et al. (2007) Immunosuppressive and anti-angiogenic sphingosine 1-phosphate receptor-1 agonists induce ubiquitinylation and proteasomal degradation of the receptor. *J Biol Chem* 282:9082–9089.
16. Michaud J, Im DS, Hla T (2010) Inhibitory role of sphingosine 1-phosphate receptor 2 in macrophage recruitment during inflammation. *J Immunol* 184: 1475–1483.

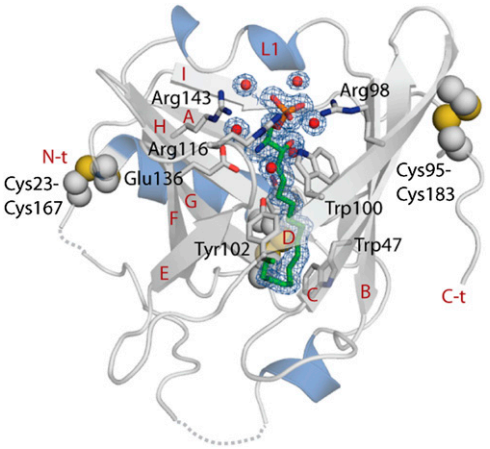

Fig. S1. The ApoM–S1P complex reveals the ligand-binding pocket. Crystal structure of apoM in complex with S1P at 1.7-Å resolution. S1P is shown as green sticks together with interacting residues. Secondary structure elements are labeled in red, and the interacting residues are labeled in black. Water molecules are shown as red spheres. Electron density for S1P and surrounding water molecules is contoured at 1 σ and colored blue. The disulfide bonds are shown as spheres and colored yellow. Unmodeled loops toward the N terminus are shown as broken lines.

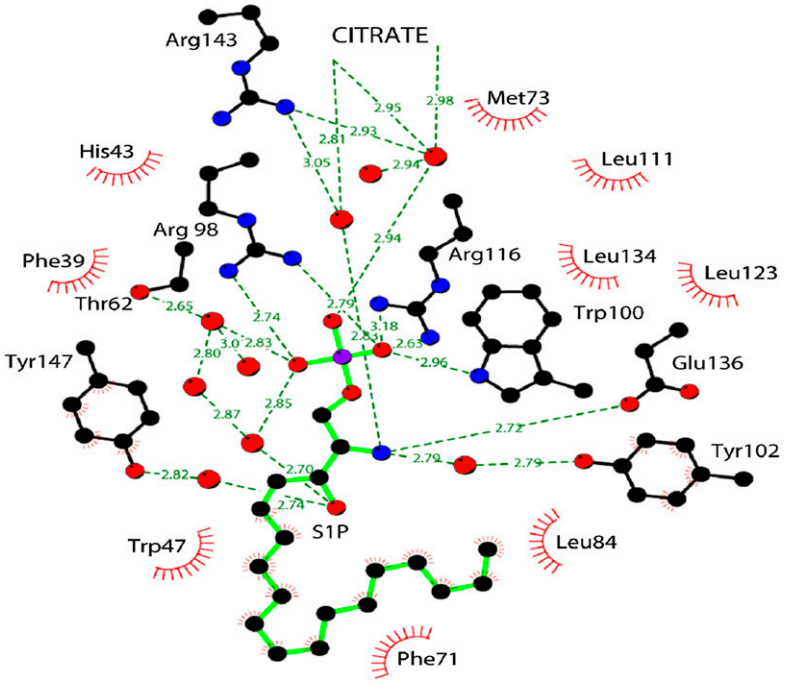

Fig. S2. LIGPLOT diagram showing S1P interactions with apoM. LIGPLOT diagram summarizing the interactions (hydrogen bonds are shown in green, and nonbonded contacts are shown in red) between S1P (green), apoM residues (black), water molecules (red), and citrate (from the crystallization buffer).

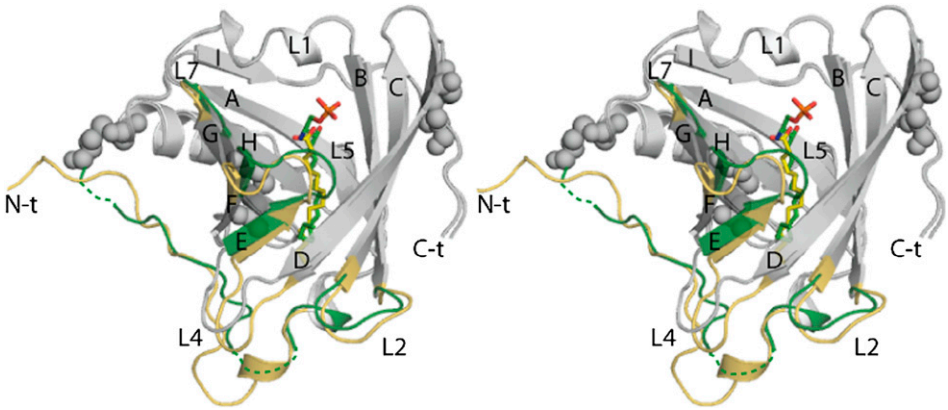

Fig. S3. ApoM–S1P complex superposed onto apoM in complex with myristic acid. In this stereographic illustration, regions of major conformational flexibility are highlighted in green (S1P complex) and yellow (myristic acid complex). Conformational rearrangements in these regions might provide alternative portals for the release of the ligand upon membrane and/or receptor association.

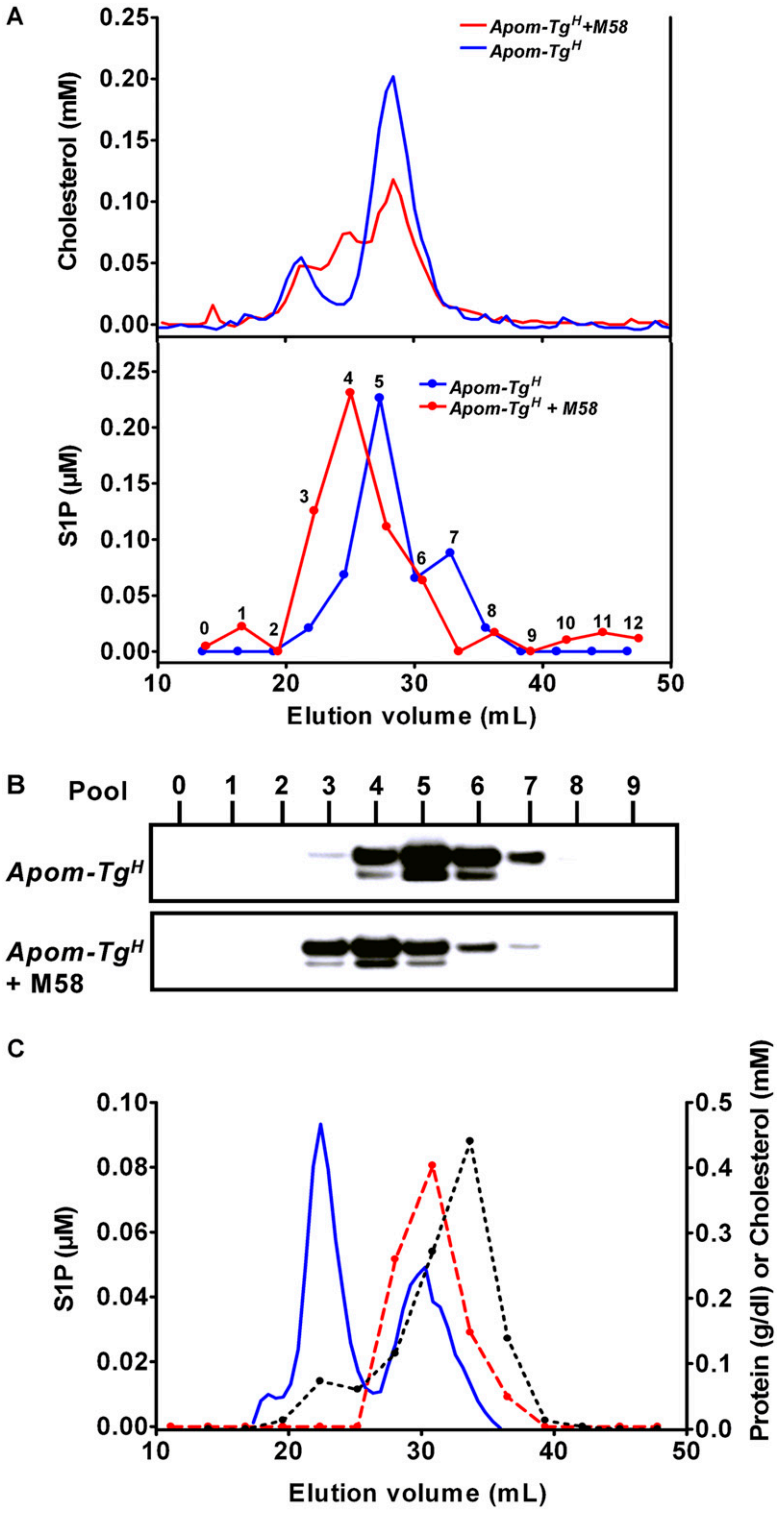

Fig. S4. S1P is bound in human apoM-containing HDL in ApoM-transgenic mice. Plasma from *Apom-Tg*^{H} mice was analyzed directly or incubated with 600 μg of a monoclonal antibody against human apoM (M58) before gel filtration analysis as described in the legend for Fig. 2. (*A*) Cholesterol profiles of *Apom-Tg*^{H} plasma with (blue line) or without (red line) preincubation with M58. Note the M58-induced increase in the size of cholesterol-containing HDL particles. S1P was determined in the gel filtration pools indicated. (*B*) Consecutive gel filtration fractions were collected in pools, and human apoM was visualized with Western blotting. Note the M58-induced increase in the size of the particles containing human apoM after preincubation with M58. (*C*) A pool of human plasma from 10 healthy individuals was subjected to gel filtration on serially connected Superose 6 and 12 columns. The flow rate was 0.4 mL/min. Fractions of 275 μL were collected. Aliquots of 10 consecutive fractions were pooled before measuring S1P (filled red symbols) and protein (dotted black line). Cholesterol concentration (solid blue line) was determined in each fraction. S1P eluted mainly in HDL- and albumin-containing fractions but not in LDL-containing fractions. The recovery of S1P was 108%.

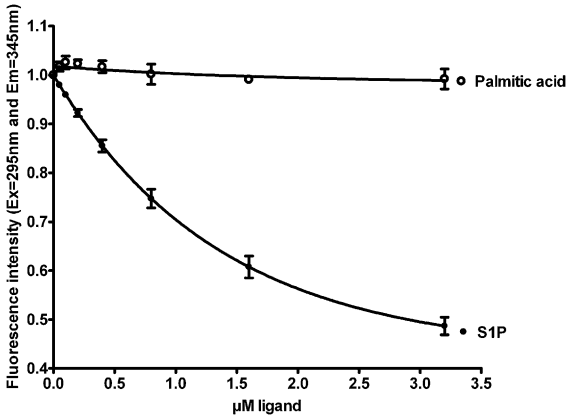

Fig. S5. S1P quenches the intrinsic fluorescence of mouse r-apoM. A truncated mouse r-apoM containing the lipocalin domain but lacking the hydrophobic signal peptide was produced in *Escherichia coli*. The r-apoM (0.7 μM) was incubated with increasing concentrations of S1P (final concentration: 0–3.2 μmol/L). The intrinsic fluorescence of apoM was measured with excitation at 295 nm and emission at 345 nm. The data are mean ± SEM (n = 3).

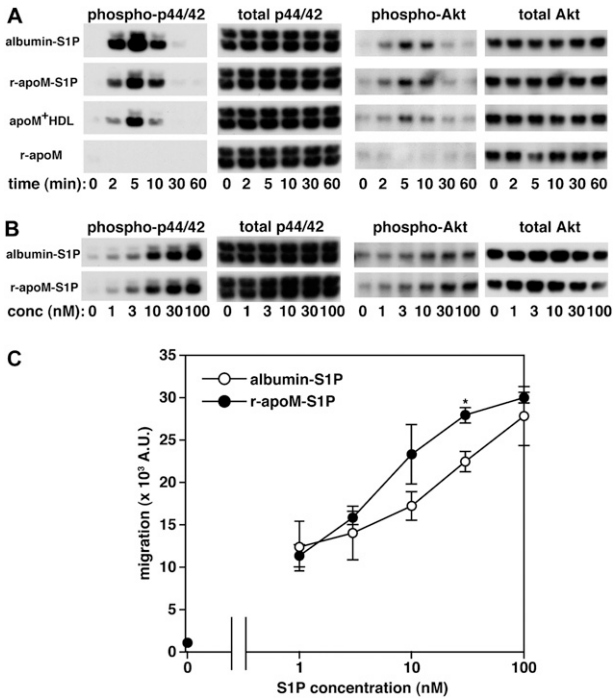

Fig. S6. ApoM-bound S1P activates $S1P_1$-mediated intracellular signaling pathways and affects migration of HUVEC. HUVEC were serum starved and stimulated for 5 min with 30 nM albumin-S1P, r-apoM–S1P, 10 μg/mL $ApoM^+$ HDL, or 30 nM S1P-free r-apoM (*A*) or with increasing concentrations of albumin- or r-apoM–S1P (*B*). Activation of p44/42 and Akt was examined by Western blot analysis using phospho-specific antibodies. (*C*) HUVEC were serum starved and subjected to migration assay with increasing concentrations of albumin- or r-apoM–S1P. Data are mean ± SD (n = 3). *$P < 0.01$.

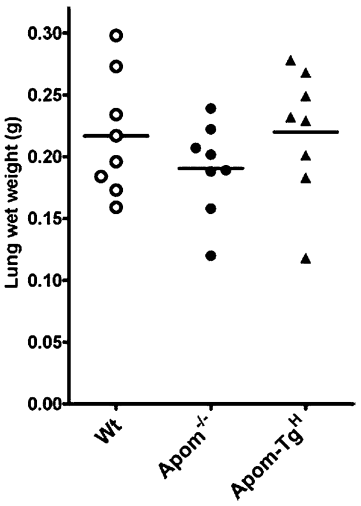

Fig. S7. Decreased lung endothelial barrier does not cause lung edema. WT, *Apom*$^{-/-}$, and *Apom-Tg*^{H} mice were i.v. injected with Evans Blue. After 30 min the mice were perfused with saline, and the wet weight of the lung was measured. Each point represents data from one mouse; horizontal lines indicate means.

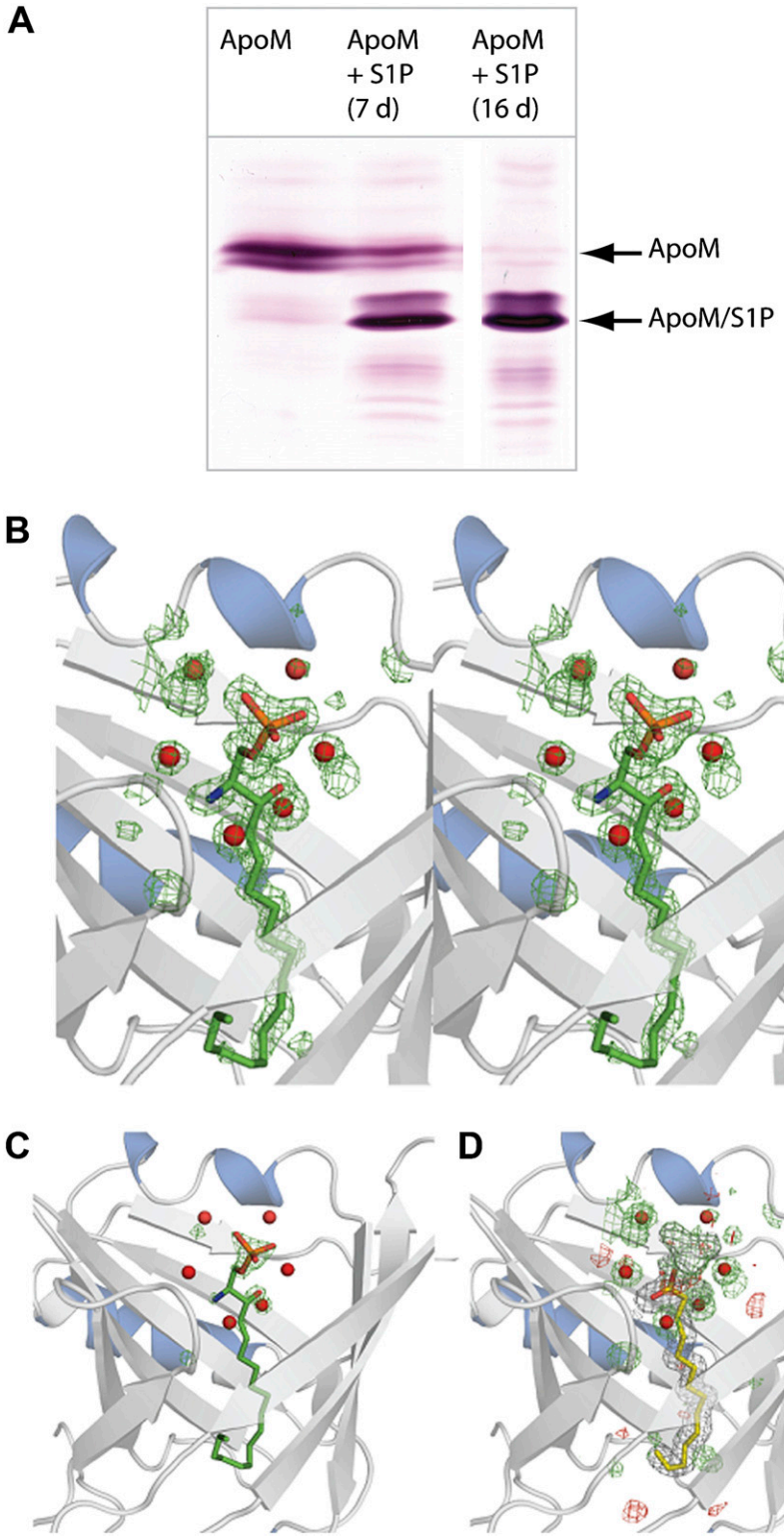

Fig. S8. Isoelectric focusing gel showing the formation of the apoM–S1P complex and crystallographic identification of the bound ligand. (*A*) Isoelectric focusing gel showing (from left to right) lane 1: apoM in complex with myristic acid (labeled as ApoM); lanes 2 and 3: apoM–S1P complex formation after apoM is incubated with S1P for 7 and 16 d, respectively. (*B*) Stereo representation of a difference Fourier map calculated after refinement of the model with the ligand S1P and all water molecules omitted during the refinement. The electron density is contoured at 3.0 σ within a radius of 5 Å of the positions of the S1P atoms. In this omit map the highest positive-density values are observed at the positions of the phosphor atoms of the two S1P molecules present in the crystallographic asymmetric unit with values of >14 σ for S1P bound to chain A and >10 σ for chain B. (C) Difference Fourier omit map contoured at 6 σ. (*D*) Crystallographic refinement with myristic acid in the binding pocket shows clear unaccounted positive-difference density at the position of the phosphate group of S1P.

Table S1. Data collection and refinement statistics

Data collection statistics	
Wavelength (Å)	0.9184
X-ray source	Bessy Synchrotron
Detector	MarCCD (165 mm)
Space group	$P3_121$
Unit cell parameters	a = b = 68.28 Å, c = 135.58 Å $\alpha = \beta = 90°$, $\gamma = 120°$
Matthews coefficient($Å^3/Da^{-1}$)	2.46
Molecules/asymmetric unit	2
Solvent content	49.98
Resolution (Å)*	1.7 (1.7–1.74)
No. of reflections (unique)	40,599 (2,949)
Redundancy*	6.07 (6.18)
Completeness (%)*	98.9 (98.3)
Mean I/(σI)*	15.55 (3.34)
R_{sym} (%)*	6.9 (63.7)
Wilson B-factor ($Å^2$)	29.02
Refinement statistics	
Final R-factor (%)	
Working set	19.08
Working set + test set	19.23
Final free R-factor (%)†	22.08
Rms deviations	
Bond lengths (Å)	0.012
Bond angles (°)	1.414
Mean B-value ($Å^2$)	
Protein	30.67
S1P; citrate	24.41;22.98
Solvent	21.38
No. of protein atoms	2501
No. of S1P atoms; citrate atoms	50; 13
No. of solvent atoms	200
Ramachandran plot (%; favored/allowed/outlier)	99.3/0.7/0

*Numbers in parenthesis are for the highest-resolution shell.

†Five percent of reflections have been chosen as R_{free} set. R_{sym} is calculated as $\sum_n \sum_i |I_i - < I >| / \sum_n \sum_i < I >$ where I_i is the i^{th} observation of the n^{th} reflection and $<I>$ is the mean of all observations of the n^{th} reflection.